Direct Detection of Dark Matter in the MSSM with Non-Universal Higgs Masses

John Ellis[1], **Andy Ferstl**[2], **Keith A. Olive**[3] and **Yudi Santoso**[3]

[1] *TH Division, CERN, Geneva, Switzerland*

[2] *Department of Physics, Winona State University, Winona, MN 55987, USA*

[3] *William I. Fine Theoretical Physics Institute,*

University of Minnesota, Minneapolis, MN 55455, USA

Abstract

We calculate dark matter scattering rates in the minimal supersymmetric extension of the Standard Model (MSSM), allowing the soft supersymmetry-breaking masses of the Higgs multiplets, $m_{1,2}$, to be non-universal (NUHM). Compared with the constrained MSSM (CMSSM) in which $m_{1,2}$ are required to be equal to the soft supersymmetry-breaking masses m_0 of the squark and slepton masses, we find that the elastic scattering cross sections may be up to two orders of magnitude larger than values in the CMSSM for similar LSP masses. We find the following preferred ranges for the spin-independent cross section: 10^{-6} pb $\gtrsim \sigma_{SI} \gtrsim 10^{-10}$ pb, and for the spin-dependent cross section: 10^{-3} pb $\gtrsim \sigma_{SD}$, with the lower bound on σ_{SI} dependent on using the putative constraint from the muon anomalous magnetic moment. We stress the importance of incorporating accelerator and dark matter constraints in restricting the NUHM parameter space, and also of requiring that no undesirable vacuum appear below the GUT scale. In particular, values of the spin-independent cross section another order of magnitude larger would appear to be allowed, for small $\tan\beta$, if the GUT vacuum stability requirement were relaxed, and much lower cross-section values would be permitted if the muon anomalous magnetic moment constraint were dropped.

1 Introduction

There have been many previous studies of the elastic scattering rates of supersymmetric relic particles on matter in the minimal supersymmetric extension of the Standard Model (MSSM) [1] - [6], assuming conservation of $R \equiv (-1)^{3B+L+2S}$, where B is the baryon number, L the lepton number and S the spin, so that the lightest supersymmetric particle (LSP) is absolutely stable. As in most previous studies, we assume this to be the lightest neutralino χ [7]. In this paper, we refine and extend previous calculations of the elastic scattering rates when the input soft supersymmetry-breaking scalar masses for the Higgs multiplets are allowed to be non-universal at the input GUT scale, the non-universal Higgs model (NUHM).

As we discuss later in more detail, it is important to impose the constraints due to accelerator experiments, including searches at LEP, $b \to s\gamma$ and (optionally) the muon anomalous magnetic moment, $g_\mu - 2$. We assume also that most of the cold dark matter is composed of LSPs, with relic density $0.1 < \Omega_\chi h^2 < 0.3$, while being aware that the lower part of this range currently appears the most plausible [8].

In the constrained MSSM (CMSSM), in which all the soft supersymmetry-breaking scalar masses m_0 are assumed to be universal, including those for the Higgs doublets $H_{1,2}$, the underlying parameters may be taken as m_0, the soft supersymmetry-breaking gaugino mass $m_{1/2}$ which is assumed to be universal, the trilinear supersymmetry-breaking parameters A_0 that we set to zero at the GUT scale in this paper, and the ratio $\tan\beta$ of Higgs vacuum expectation values. In the NUHM [9] - [13], there are two additional free parameters, the two soft Higgs masses or equivalently the Higgs superpotential coupling μ and the pseudoscalar Higgs boson mass m_A. These would be fixed by the electroweak symmetry-breaking vacuum conditions in the CMSSM, up to a sign ambiguity in μ, in terms of the other parameters $(m_0, m_{1/2}, A_0, \tan\beta)$. We use the parameters $(m_0, m_{1/2}, \mu, m_A, A_0, \tan\beta)$ to parametrize the more general NUHM.

As we have pointed out previously [12, 13], this six-dimensional NUHM parameter space is significantly restricted by the requirement that no undesirable vacuum appears when one uses the renormalization-group equations to run the soft supersymmetry-breaking parameters between the input GUT scale and the electroweak scale. This requirement constrains the non-universalities of the Higgs masses: $\hat{m}_i \equiv \text{sign}(m_i^2)|m_i/m_0| : i = 1, 2$, which in turn restricts the range of elastic scattering cross sections that we find [1].

---

[1] This extended stability requirement would also exclude non-universalities for the input squark and slepton masses that allowed their physical values to be similar, an assumption that might lead to much larger elastic scattering cross sections than we find here.

The allowed regions in the (μ, m_A), (μ, M_2) and $(m_{1/2}, m_0)$ planes for certain discrete values of the other NUHM parameters have been described in [13]. Our first step in this paper is to provide contours of the elastic scattering cross sections in selected planes, providing a first comparison with the CMSSM points that appear in these planes. Secondly, we display the ranges of elastic scattering cross sections that are allowed in these planes, as functions of the LSP mass. In general, we find that the spin-independent elastic scattering cross sections may be up to two orders of magnitude larger than values in the CMSSM for similar LSP masses, and another order of magnitude larger if the GUT vacuum stability requirement is relaxed. Thirdly, we display ranges of the elastic scattering cross sections as functions of the LSP mass for all allowed values of the other NUHM parameters.

We review the NUHM in Section 2, including the experimental and phenomenological constraints on its parameter space. Then, in Section 3, we summarize our treatment of the elastic scattering matrix elements and display contours of the cross sections in various planar projections of the NUHM parameter space. Section 4 presents and discusses the ranges of the cross sections attainable in the NUHM. Finally, Section 5 draws some conclusions from our analysis.

2 The NUHM and Constraints on its Parameter Space

We assume that the soft supersymmetry-breaking parameters are specified at some large input scale M_X, such as the supergravity or grand unification scale. Motivated by restrictions on flavour-changing neutral interactions, we assume that squarks and sleptons with the same Standard Model quantum numbers have universal soft supersymmetry-breaking scalar masses at this input scale. With the weaker justification provided by some GUTs, we further assume universality between the soft scalar masses of squarks and sleptons. However, in the NUHM studied here, we allow the soft supersymmetry-breaking scalar contributions to the masses of the Higgs supermultiplets at M_X to be free non-universal parameters. Their running from M_X down to low energies relates $m_1^2(M_X)$ and $m_2^2(M_X)$ to the Higgs supermultiplet mixing parameter μ and the pseudoscalar Higgs mass m_A. Therefore, we use as free parameters $\mu(m_z) \equiv \mu$ and $m_A(Q) \equiv m_A$, where $Q \equiv (m_{\widetilde{t}_R} m_{\widetilde{t}_L})^{1/2}$, in addition to the parameters $(m_0(M_X), m_{1/2}(M_X), A_0, \tan\beta)$ used in the CMSSM [2].

The electroweak vacuum conditions may be written in the form:

$$m_A^2(Q) = m_1^2(Q) + m_2^2(Q) + 2\mu^2(Q) + \Delta_A(Q) \tag{1}$$

[2]In this paper, we use the input $A_0 = 0$ for definiteness, noting that the range of effective low-energy values of A, after renormalization below the GUT scale, is quite limited.

and

$$\mu^2 = \frac{m_1^2 - m_2^2 \tan^2 \beta + \frac{1}{2} m_z^2 (1 - \tan^2 \beta) + \Delta_\mu^{(1)}}{\tan^2 \beta - 1 + \Delta_\mu^{(2)}}, \tag{2}$$

where Δ_A and $\Delta_\mu^{(1,2)}$ are loop corrections [14, 15, 16] and $m_{1,2} \equiv m_{1,2}(m_z)$. We incorporate the known radiative corrections [14, 17, 18] c_1, c_2 and c_μ relating the values of the NUHM parameters at Q to their values at m_z:

$$
\begin{aligned}
m_1^2(Q) &= m_1^2 + c_1 \\
m_2^2(Q) &= m_2^2 + c_2 \\
\mu^2(Q) &= \mu^2 + c_\mu .
\end{aligned}
\tag{3}
$$

Solving for m_1^2 and m_2^2, one has

$$
\begin{aligned}
m_1^2(1 + \tan^2 \beta) &= m_A^2(Q) \tan^2 \beta - \mu^2(\tan^2 \beta + 1 - \Delta_\mu^{(2)}) - (c_1 + c_2 + 2c_\mu) \tan^2 \beta \\
&\quad - \Delta_A(Q) \tan^2 \beta - \frac{1}{2} m_z^2 (1 - \tan^2 \beta) - \Delta_\mu^{(1)}
\end{aligned}
\tag{4}
$$

and

$$
\begin{aligned}
m_2^2(1 + \tan^2 \beta) &= m_A^2(Q) - \mu^2(\tan^2 \beta + 1 + \Delta_\mu^{(2)}) - (c_1 + c_2 + 2c_\mu) \\
&\quad - \Delta_A(Q) + \frac{1}{2} m_z^2 (1 - \tan^2 \beta) + \Delta_\mu^{(1)},
\end{aligned}
\tag{5}
$$

which we use to perform our numerical calculations.

It can be seen from (4) and (5) that, if m_A is too small or μ is too large, then m_1^2 and/or m_2^2 can become negative and large. This could lead to $m_1^2(M_X) + \mu^2(M_X) < 0$ and/or $m_2^2(M_X) + \mu^2(M_X) < 0$, thus triggering electroweak symmetry breaking at the GUT scale. The requirement that electroweak symmetry breaking occurs far below the GUT scale forces us to impose the conditions $m_1^2(M_X) + \mu(M_X), m_2^2(M_X) + \mu(M_X) > 0$ as extra constraints, which we call the GUT stability constraint [3]. We have discussed in [13] issues related to the NUHM renormalization group equations (RGE's) and their solutions.

We assume that R parity is conserved, so that the LSP is stable and is present in the Universe today as a relic from the Big Bang. Searches for anomalous heavy isotopes tell us that the dark matter should be weakly-interacting and neutral, and therefore eliminate all but the neutralino and the sneutrinos as possible LSPs. LEP and direct dark-matter searches together exclude a sneutrino LSP [20], at least if the majority of the CDM is the LSP. Thus we require in our analysis that the lightest neutralino be the LSP. We include in

---

[3] For a different point of view, however, see [19].

our analysis all relevant coannihilation processes involving this LSP and sparticles that may become near-degenerate in various regions of the NUHM parameter space. We restrict our attention to regions of the NUHM parameter space where $0.1 < \Omega_\chi h^2 < 0.3$.

We impose in our analysis the constraints provided by direct sparticle searches at LEP, including that on the lightest chargino $\chi^\pm$: $m_{\chi^\pm} \gtrsim 103.5$ GeV [21], and that on the selectron $\tilde{e}$: $m_{\tilde{e}} \gtrsim 99$ GeV [22]. Another important constraint is provided by the LEP lower limit on the Higgs mass: $m_H > 114.4$ GeV [23] in the Standard Model[4]. The lightest Higgs boson h in the general MSSM must obey a similar limit, which may in principle be relaxed for larger $\tan\beta$. However, as we discussed in our previous analysis of the NUHM [12], the relaxation in the LEP limit is not relevant in the regions of MSSM parameter space of interest to us. We recall that m_h is sensitive to sparticle masses, particularly $m_{\tilde{t}}$, via loop corrections [24, 25], implying that the LEP Higgs limit constrains the NUHM parameters. We also impose the constraint imposed by measurements of $b \to s\gamma$ [26], as discussed in [13].

We take an agnostic attitude towards the latest value of the anomalous magnetic moment of the muon reported [27] by the BNL E821 experiment. The world average of $a_\mu \equiv \frac{1}{2}(g_\mu - 2)$ now deviates by $(33.7 \pm 11.2) \times 10^{-10}$ from the Standard Model calculation of [28] using $e^+ e^-$ data, and by $(9.4 \pm 10.5) \times 10^{-10}$ from the Standard Model calculation of [28] based on τ decay data. On some of the subsequent plots, we display the formal 2-σ range $11.3 \times 10^{-10} < \delta a_\mu < 56.1 \times 10^{-10}$. However, in view of the chequered history of the theoretical Standard Model calculations of a_μ, we do not impose this as an absolute constraint on the supersymmetric parameter space.

The results of applying the above constraints to various two-dimensional projections of the NUHM parameter space were described in [13].

3   Contours of the Cross Sections for Elastic Scattering

The code we use to calculate the spin-independent and -dependent elastic dark matter scattering cross sections $\sigma_{SI,SD}$ was documented in [2, 3], together with the ranges of values of the hadronic matrix elements that we use. The cross sections for protons and neutrons are similar within the quoted uncertainties in these matrix elements. There are other codes available [29] that include additional contributions to the scattering matrix elements, but a comparison [4] showed that the improvements were not essential for the CMSSM, and we believe they may also be neglected for our comparisons of the NUHM.

---

[4]In view of the theoretical uncertainty in calculating m_h, we apply this bound with just three significant digits, i.e., our figures use the constraint $m_h > 114$ GeV.

In [13], we analyzed NUHM dark matter in two ways: (i) fixing $\tan\beta = 10$ and $\mu > 0$, but choosing different values of μ and m_A, rather than assuming the CMSSM values, and (ii) varying $\tan\beta$ for representative fixed values of μ and m_A. We presented in [13] three types of slices through the NUHM parameter space, along $(m_{1/2}, m_0)$ planes, (μ, m_A) planes and (μ, M_2) planes.

In this paper, we concentrate first on a few specific examples of these slices, presenting later more general results. We choose two representative examples each of the $(m_{1/2}, m_0)$ planes, (μ, m_A) planes and (μ, M_2) planes shown previously. As we discuss later in more detail, the dependences of the cross sections on $\tan\beta$ are weaker than those on some other parameters, so we concentrate on planes for $\tan\beta = 10$. The examples we choose are the $(m_{1/2}, m_0)$ planes for $\mu = 400$ GeV, $m_A = 400$ GeV and $\mu = 700$ GeV, $m_A = 700$ GeV, corresponding to Figs. 2(a) and (d) of [13], the (μ, m_A) planes for $m_0 = 100$ GeV, $m_{1/2} = 300$ GeV and $m_0 = 300$ GeV, $m_{1/2} = 300$ GeV, corresponding to Figs. 4(a) and (c) of [13], and the (μ, M_2) planes for $m_0 = 100$ GeV, $m_A = 300$ GeV and $m_0 = 300$ GeV, $m_A = 500$ GeV, corresponding to Figs. 8(a) and (c) of [13].

3.1   Examples of $(m_{1/2}, m_0)$ Planes

We display in Fig. 1 contours of (a,b) the spin-independent and (c,d) the spin-dependent elastic scattering cross sections, in the cases $\tan\beta = 10$, and (a,c) $\mu = 400$ GeV and $m_A = 400$ GeV, and (b,d) $\mu = 700$ GeV and $m_A = 700$ GeV. We assume here and in the subsequent figures that $A_0 = 0$, $m_t = 175$ GeV and $m_b(m_b)^{\overline{MS}}_{SM} = 4.25$ GeV. Here and elsewhere, the thickest contours denote decades in the cross-section values in pb, labelled by their exponents. The medium and thinnest lines are intermediate contours in the cross-section values, namely $2\times$ and $5\times$ decades, as labelled.

We notice immediately that the cross-section contours are nearly vertical at large $m_{1/2}$, reflecting the fact that they become almost independent of m_0 in the NUHM. We also notice that, within the GUT stability range (inside the black dot-dashed curves), the cross sections *increase* with $m_{1/2}$. This is because the LSP becomes more Higgsino-like as $m_{1/2}$ increases. However, the cross sections do decrease again for very large $m_{1/2}$ beyond the GUT stability limit as the low energy scalar masses increase with $m_{1/2}$ as does the light Higgs mass (though slowly).

The GUT stability requirement imposes $m_{1/2} \lesssim 600(1100)$ GeV in panels (a,c) and (b,d), respectively. Because of the increases in the cross sections with $m_{1/2}$, there are in turn *upper bounds* on the cross sections, that would not be respected if GUT stability were disregarded.
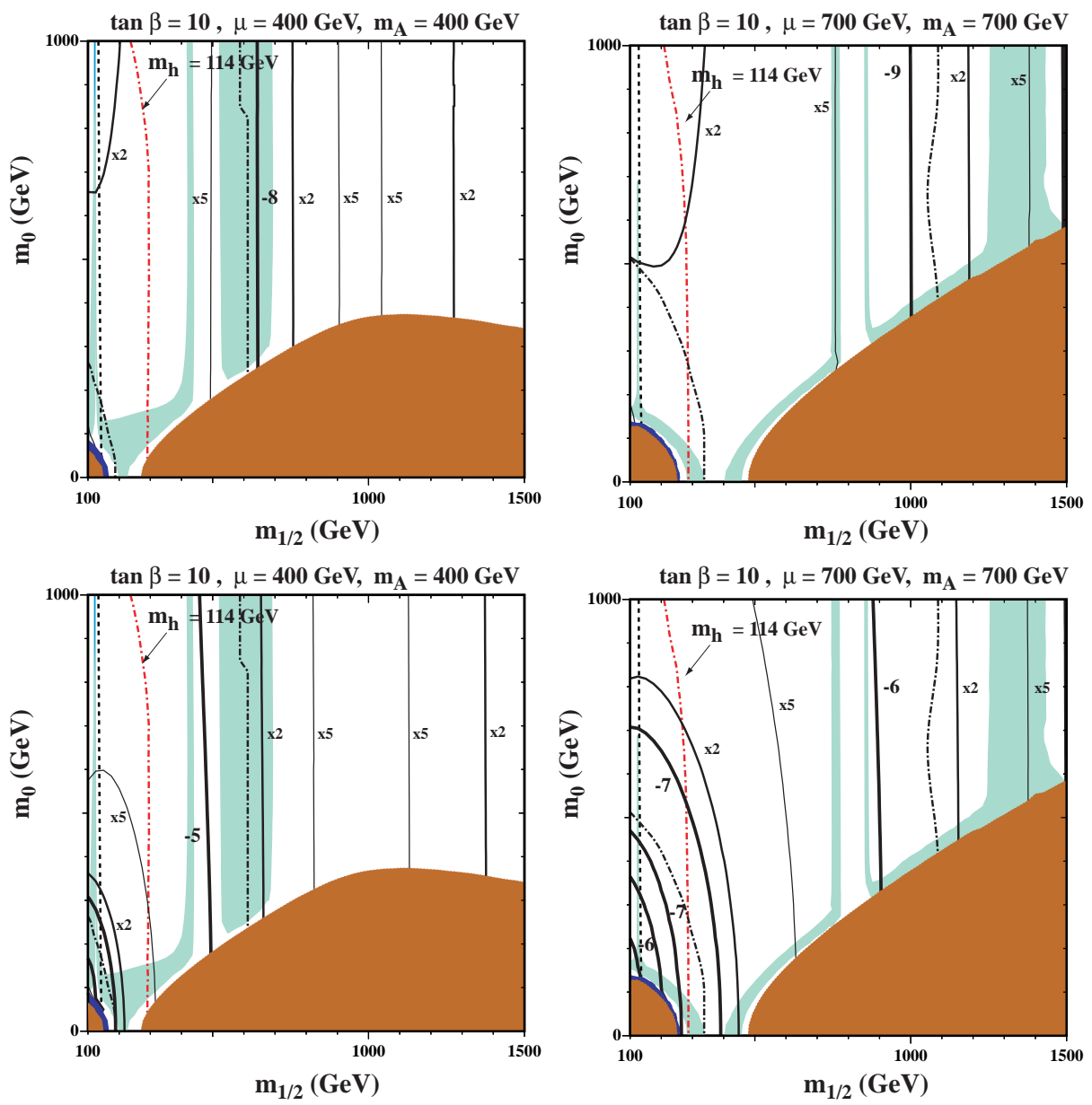
Figure 1: *Contours of (a,b) the spin-independent and (c,d) the spin-dependent cross sections (solid black lines) are superimposed on the NUHM $(m_{1/2}, m_0)$ planes for $\tan\beta = 10$ and (a,c) $\mu = 400$ GeV and $m_A = 400$ GeV, and (b,d) $\mu = 700$ GeV and $m_A = 700$ GeV. The near-vertical (red) dot-dashed lines are the contours $m_h = 114$ GeV, and the near-vertical (black) dashed lines at lower $m_{1/2}$ are the contours $m_{\chi^\pm} = 103.5$ GeV. The dark (brick red) shaded regions is excluded because a charged particle is lighter than the neutralino, and the darker (dark blue) shaded regions is excluded because the LSP is a sneutrino. The light (turquoise) shaded areas are the cosmologically preferred regions with $0.1 \leq \Omega_\chi h^2 \leq 0.3$. The dark (black) dot-dashed lines indicate the GUT stability constraint. There are two such lines for each panel and only the areas in between are allowed by this constraint.*

6

Because the $g_\mu - 2$ constraint would provide even stronger upper bounds on $m_{1/2}$, it would also impose stronger upper bounds on the cross sections. In Figs. 1 - 3, we have left off the $g_\mu - 2$ contours to avoid confusion with the cross section contours we are highlighting here. For the case with $\mu = 400$ GeV and $m_A = 400$ GeV, the $g_\mu - 2$ constraint places an upper limit on $m_{1/2}$ of about 400 GeV and for the case with $\mu = 700$ GeV and $m_A = 700$ GeV, the limit is $m_{1/2} \lesssim 450$ GeV.

As already remarked, the cross sections themselves do not vary greatly with $\tan\beta$, but the interplay of the other constraints is rather $\tan\beta$-dependent. In particular, at large $\tan\beta$ the $g_\mu - 2$ constraint would not reduce significantly the upper bounds on the cross sections.

3.2 Examples of (μ, m_A) Planes

We display in Fig. 2 contours of (a,b) the spin-independent and (c,d) the spin-dependent elastic scattering cross sections, in the cases $\tan\beta = 10$, and (a,c) $m_0 = 100$ GeV and $m_{1/2} = 300$ GeV, (b,d) $m_0 = 300$ GeV and $m_{1/2} = 300$ GeV. We see that there are large suppressions in the spin-independent cross section for $\mu \sim -100$ GeV and $m_A \gtrsim 500$ GeV, reflecting a cancellation in the matrix element. Apart from this, the cross sections generally decrease with increasing $|\mu|$ and (to a lesser extent) m_A. In this sense, the lower bounds on $|\mu|$ and m_A set an upper bound on the cross section in the allowed region.

In the CMSSM, cancellations which drive the cross section to extremely small values occur only in the spin-independent case, and only for $\mu < 0$. In the NUHM model, however, we find that there is a new source for a cancellation which affects the spin-dependent cross section for either sign of μ. The reason this occurs is as follows. In the CMSSM, the spin-dependent cross section is dominated by the up-squark exchange term and, despite the difference in the relative signs of the up-type and down-type contributions, the total cross section remains reasonably large. On the other hand, in the NUHM case considered here, low-energy sfermion masses are affected by the splitting between the soft supersymmetry-breaking Higgs masses at the GUT scale, $S = g_1^2(m_1^2 - m_2^2)/4$. When $S \neq 0$, the up squarks get somewhat heavier and the down squarks somewhat lighter as S increases (see [13] for details on the effects of S in the renormalization-group equations), opening up the possibility of a cancellation between the contributions. In Fig. 2(c,d), the cancellation occurs between the two 10^{-7} pb contours very close to, but outside the GUT stability curve. The GUT stability requirement, that bounds $|\mu| \lesssim 700$ GeV in the figures displayed, therefore provides *lower bounds* on the spin-dependent cross sections. These are somewhat lower than the values found at the CMSSM points indicated by crosses in Fig. 2. The same cannot be said for the

7

spin-independent cross-sections, because the very small cross sections due to cancellations occur within the GUT stability region, except when one applies the $g_\mu - 2$ constraint, which excludes the $\mu < 0$ region. The interplay of the other constraints is more complicated: as usual, $\mu < 0$ is disfavoured by the m_h, $b \to s\gamma$ and $g_\mu - 2$ constraints. The upshot for $\mu > 0$ is that the cross sections are bounded above by the $\Omega_\chi h^2$ constraint, so that they cannot be much more than a factor of ~ 10 greater than the CMSSM values.

For the values of parameters chosen in Fig. 2 (a,c), we obtain a spin-independent cross-section of $\sigma_{SI} = 2.6 \times 10^{-9}$ pb and a spin-dependent cross-section of $\sigma_{SD} = 5.4 \times 10^{-6}$ pb in the CMSSM for $\mu > 0$ (cf. the position of the crosses in the figures). In the NUHM, we find that the range of possible cross sections (for this case) is 3×10^{-10}pb $\lesssim \sigma_{SI} \lesssim 3 \times 10^{-8}$pb and 3×10^{-8}pb $\lesssim \sigma_{SD} \lesssim 1.6 \times 10^{-4}$pb when all constraints other than $g_\mu - 2$ are included. For the parameters in Fig. 2 (b,d), we find the CMSSM spin-independent cross section $\sigma_{SI} = 1.9 \times 10^{-9}$ pb, while the spin-dependent cross section is relatively unchanged. Note, however, that this CMSSM point would be excluded due to an excessive value for Ωh^2 (> 1). In the NUHM, this parameter choice is allowed and gives the range 10^{-9}pb $\lesssim \sigma_{SI} \lesssim 8 \times 10^{-8}$pb and 9×10^{-9}pb $\lesssim \sigma_{SD} \lesssim 2 \times 10^{-4}$pb for the elastic cross sections. In this case, there is essentially no 'bulk' cosmological region, and the spread in σ is due to the region where the relic density is due to the heavy Higgs s-channel exchange, allowing for a larger range in μ.

3.3 Examples of (μ, M_2) Planes

We display in Fig. 3 contours of (a,b) the spin-independent and (c,d) the spin-dependent elastic scattering cross sections, in the cases $\tan\beta = 10$, and (a,c) $m_0 = 100$ GeV and $m_A = 500$ GeV, (b,d) $m_0 = 300$ GeV and $m_A = 500$ GeV. Because the cross sections vary relatively rapidly, we have not included all the decade cross-section contours in panels (c,d).

We see again in this case the suppression in the spin-independent cross section for $\mu \sim -100$ GeV and $M_2 \gtrsim 200$ GeV, apart from which the cross sections decrease with increasing $|\mu|$, at least within the GUT stability region. The spin-dependent cross section, on the other hand, starts rising again at large $|\mu|$, reflecting the fact that one has traversed a cancellation in the scattering matrix element of the type described in the previous subsection. Once again, the cancellation is found between the 10^{-7} pb contours just outside the GUT stability curve.

For the values of parameters chosen in Fig. 3 (a,c), we obtain a spin-independent cross section $\sigma_{SI} = 2 \times 10^{-9}$ pb and a spin-dependent cross section $\sigma_{SD} = 3 \times 10^{-6}$ pb in the CMSSM (cf. the position of the crosses in the figures). In the NUHM, we find that the
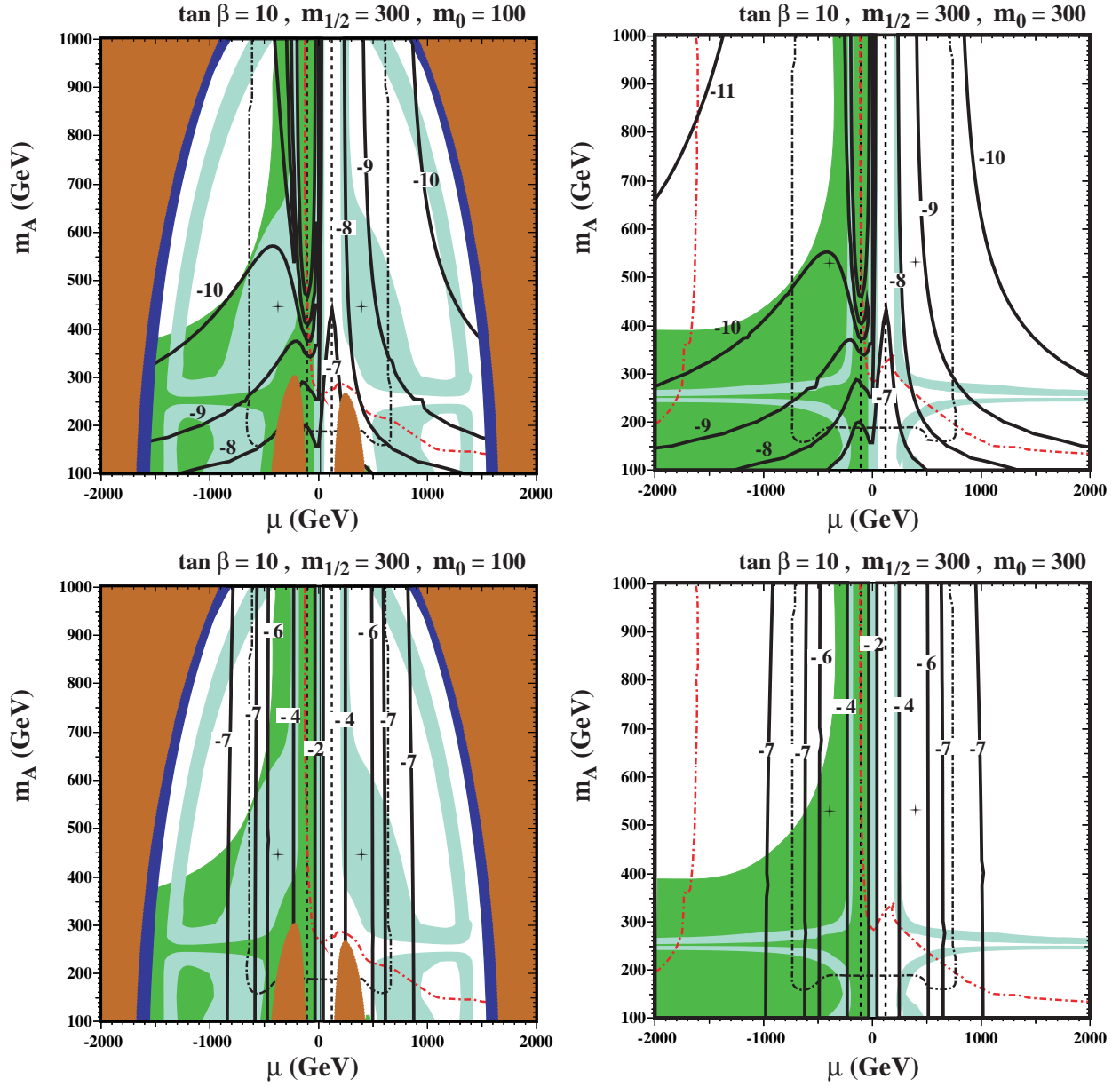
Figure 2: *Contours of (a,b) the spin-independent and (c,d) the spin-dependent cross sections (solid black lines) are superimposed on the NUHM (μ, m_A) planes for $\tan\beta = 10$, (a,c) $m_0 = 100$ GeV and $m_{1/2} = 300$ GeV, (b,d) $m_0 = 300$ GeV and $m_{1/2} = 300$ GeV. The shadings and line styles are the same as in Fig. 1. Here, we see in addition the constraint from $b \to s\gamma$. The excluded region is medium (green) shaded. The crosses denote the CMSSM points for these choices of m_0 and $m_{1/2}$.*

range of possible cross sections for this case is 2.5×10^{-11}pb $\lesssim \sigma_{SI} \lesssim 9 \times 10^{-8}$pb and 1.5×10^{-9}pb $\lesssim \sigma_{SD} \lesssim 2 \times 10^{-3}$pb. For the parameters in Fig. 2 (b,d), the CMSSM spin-independent cross section is $\sigma_{SI} = 3 \times 10^{-9}$ pb, while the spin-dependent cross section is $\sigma_{SD} = 10^{-5}$ pb. Note, however, that this CMSSM point would be excluded due to a excessive value for Ωh^2 ($\gtrsim 1$). In the NUHM, this parameter choice is allowed and gives the range 10^{-13}pb $\lesssim \sigma_{SI} \lesssim 2 \times 10^{-8}$pb and 9×10^{-9}pb $\lesssim \sigma_{SD} \lesssim 2 \times 10^{-4}$pb for the elastic cross sections.

4   Allowed Ranges of Elastic Cross Sections

Following our discussion in the previous Section of some important features in a few examples of parameter planes in the NUHM, we now display the ranges of elastic scattering cross sections permitted by various theoretical and experimental constraints. We start with the specific NUHM parameter planes discussed above, and then go on to generalize the discussion. In each of the specific planes, we show the effect on the allowed cross section when the phenomenological and cosmological constraints are applied successively. We start with the very simple requirement that the LSP be a neutralino with $m_{\chi^\pm} \gtrsim 103.5$ GeV and $m_{\tilde{e}} \gtrsim 99$ GeV. We then apply either the Higgs cut or the $b \to s\gamma$ cut. Our standard cut is defined to include these two in addition to the appropriate value for Ωh^2. Following the standard cut we apply sequentially the GUT stability constraint and the constraint due to $g_\mu - 2$.

4.1   Specific Planes

We consider first the $(m_{1/2}, m_0)$ plane for $\tan\beta = 10$ and $\mu = m_A = 400$ GeV that was displayed earlier in Fig. 1(a,c). The horizontal axes in the various panels of Fig. 4 correspond to the LSP mass m_χ, and the vertical axes show the ranges of (a,c,e) the spin-independent and (b,d,f) the spin-dependent elastic cross sections. The first row of panels (a,b) shows the ranges allowed by our cuts on the LSP (dark lines), m_h (lighter lines) and standard cut (shaded), the second row (c,d) displays the further impact of the GUT stability constraint, and the third row (e,f) implements all the cuts, including that on $g_\mu - 2$.

We see in Fig. 4(a,b) that the scattering cross sections rise monotonically with m_χ, except close to the upper limit on m_χ, reflecting the increase with $m_{1/2}$ that was already commented in connection with Fig. 1. We also note that the ranges of cross sections allowed for any fixed value of m_χ is very restricted, reflecting the fact the the contours of equal cross section in Fig. 1(a,c) are almost vertical in the parameter range of interest. The break that appears in the middle of Fig. 4(a,b), and is seen more clearly in (c,d), reflects the range of
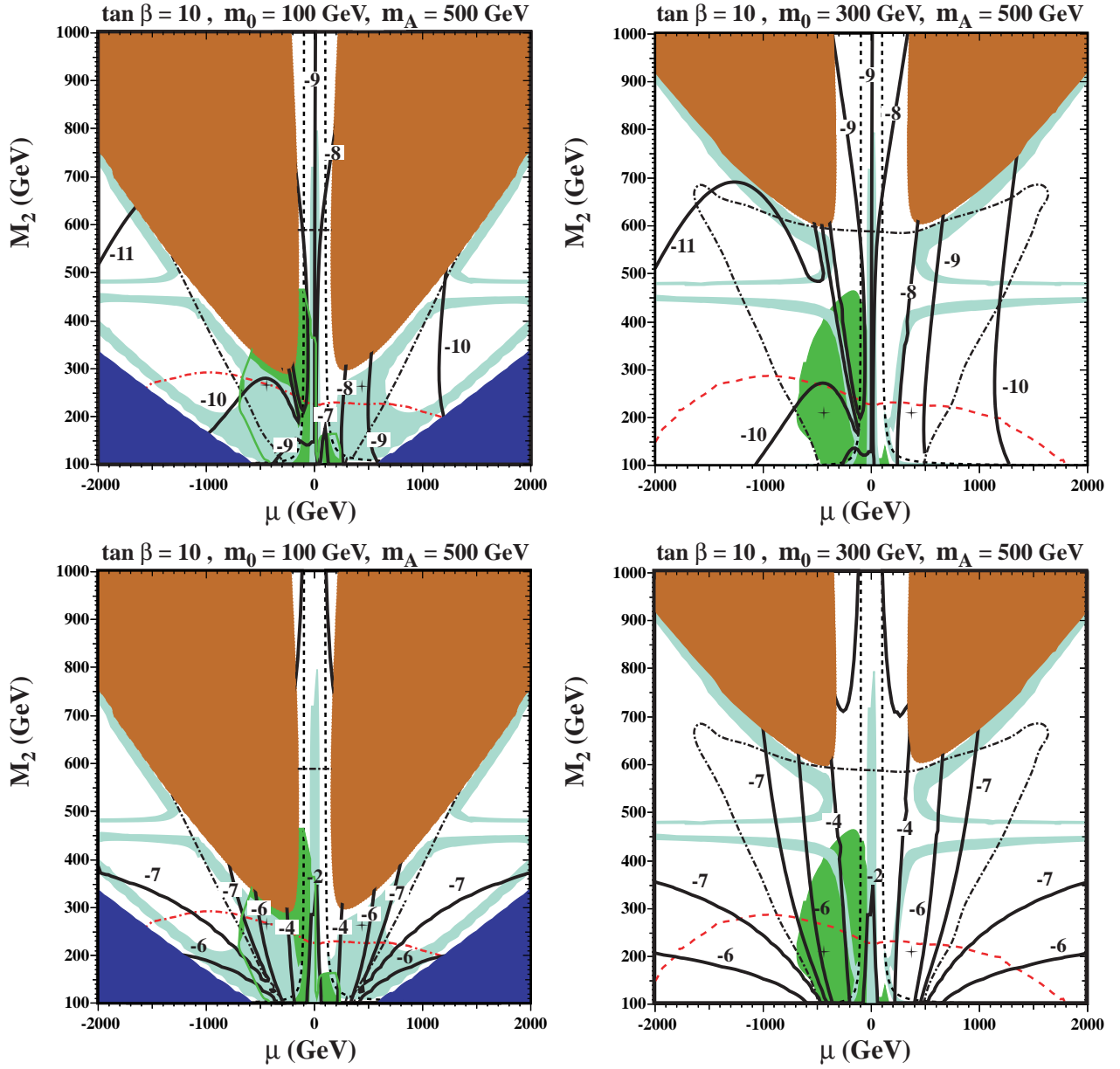
Figure 3: *Contours (a,b) of the spin-independent and (c,d) spin-dependent cross sections (solid black lines) are superimposed on the NUHM* (μ, M_2) *planes for* $\tan\beta = 10$, *(a,c)* $m_0 = 100$ *GeV and* $m_A = 500$ *GeV, (b,d)* $m_0 = 300$ *GeV and* $m_A = 500$ *GeV. The shadings and line styles are the same as in Fig. 2, and the crosses denote the CMSSM points for these choices of* m_0 *and* m_A.
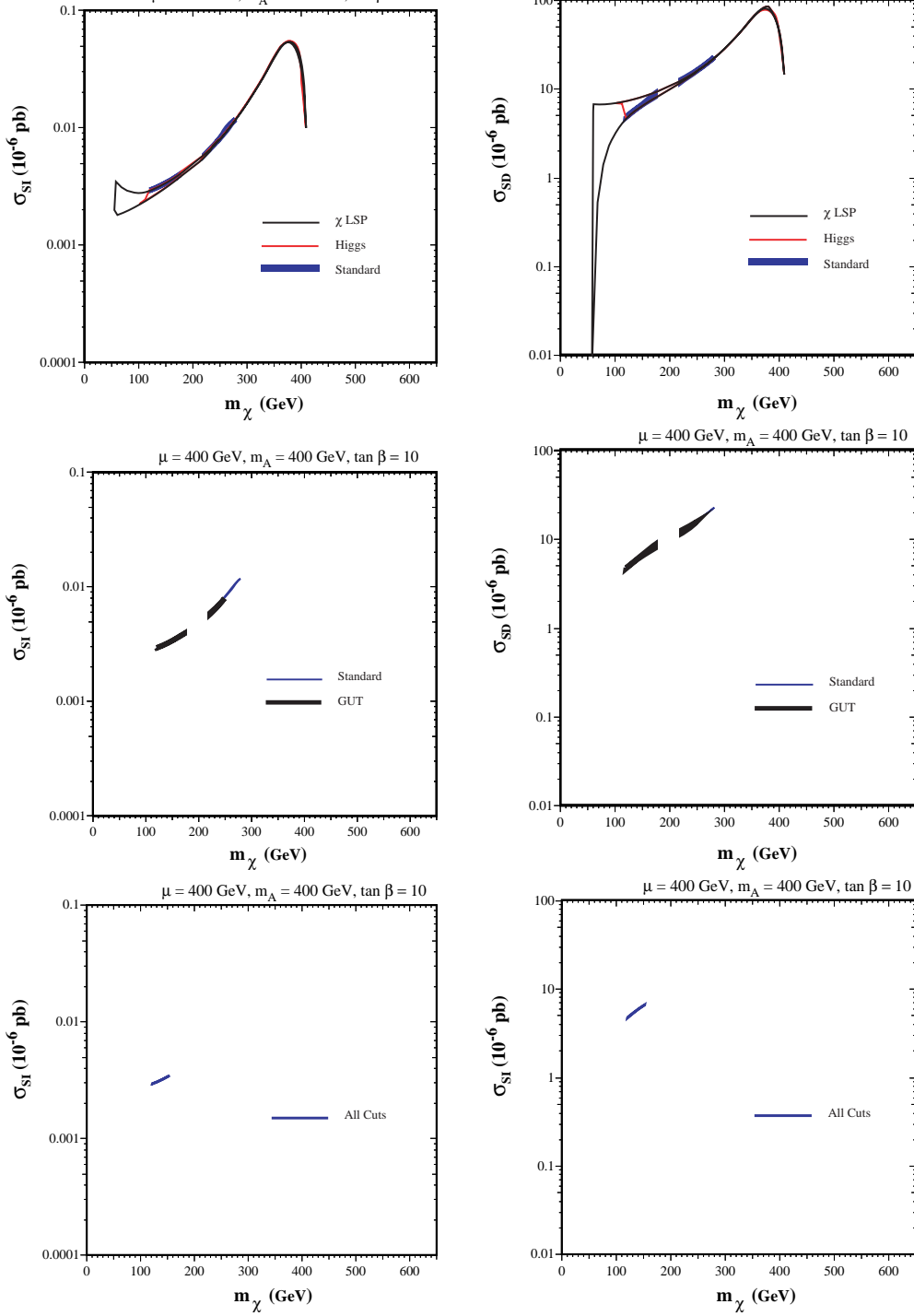
Figure 4: *Cross sections allowed in a slice through the NUHM parameter space provided by the $(m_{1/2}, m_0)$ plane for $\tan\beta = 10$ and $\mu = m_A = 400$ GeV. Panels (a,b) are with our cuts on the LSP (dark lines), m_h (lighter lines) and standard cut (shaded), panels (c,d) also have the GUT stability constraint imposed, and panels (e,f) apply all cuts, including the possible $g_\mu - 2$ constraint. The right (left) panels show the spin-(in)dependent cross section, plotted against m_χ.*

12

$m_{1/2} \sim 500$ GeV where $\Omega_\chi h^2$ is suppressed below the preferred cosmological range by rapid direct-channel $\chi\chi$ annihilation via the H, A poles.

The most relevant effect of the extra GUT and $g_\mu - 2$ constraints is to reduce the range of $m_{1/2}$ and hence m_χ. As we see in Fig. 4(c,d), the GUT stability constraint removes the points in this NUHM parameter plane that have the largest elastic scattering cross sections. Finally, as we see in Fig. 4(e,f), the $g_\mu - 2$ constraint confines our attention to points in the NUHM parameter below the rapid-annihilation channel. In this particular case, there is a narrow preferred range of the spin-independent cross section around 3×10^{-9} pb, and the preferred range of the spin-dependent cross section is around 6×10^{-6} pb.

Our second example is the (μ, m_A) plane for $\tan\beta = 10, m_{1/2} = 300$ GeV and $m_0 = 100$ GeV, displayed previously in panels (a,c) of Fig. 2. As seen in Fig. 5(a,b), when one imposes the standard $\Omega_\chi h^2, m_h$ and $b \to s\gamma$ constraints, the cross sections generally decrease with m_χ. However, in the spin-dependent case the cross section reaches a locus of near zeroes, after which it rises again. These cancellations are avoided in this case when the Higgs and $b \to s\gamma$ constraints are applied. As then seen in Fig. 5(c,d), the GUT stability constraint, which removes portions of this NUHM parameter plane at large $|\mu|$ and small m_A, strengthens in this case the lower bounds on the cross sections. The effect of the $g_\mu - 2$ constraint is less marked in this case, as seen in Fig. 5(e,f). The final allowed ranges of the cross section are considerably wider than in the previous example: $\sim 10^{-9}$ to $\sim 10^{-8}$ pb in the spin-independent case and $\sim 10^{-7}$ to $\sim 10^{-4}$ pb in the spin-dependent case.

Our final example is the (μ, M_2) plane for $\tan\beta = 10, m_0 = 100$ GeV and $m_A = 500$ GeV, shown in Fig. 6. In this case, the standard cuts allow a particularly wide range of cross sections, varying by infinite (over 3) orders of magnitude for the spin-(in)dependent case. The different regions allowed by the standard cuts reflect the different branches of parameter space in Fig. 3. We note that some of these branches are due to the differences between positive and negative μ. We also note that some of the boundaries are due to our imposed cutoff of $|\mu| \leq 2$ TeV. In particular, had we allowed for larger values of $|\mu|$, we would have found larger neutralino masses, and the lower bounds for both the Higgs and $b \to s\gamma$ cuts (which differ for positive and negative μ) would also have been lowered. The general tendency of the standard cuts is to decrease the cross sections with increasing m_χ, though with considerable variation. The GUT stability constraint in this case removes a region at large M_2 and hence m_χ, that removes the points with the lowest cross sections. This effect is particularly marked for the spin-dependent case, where the range is now reduced to (a mere) 5 orders of magnitude. The $g_\mu - 2$ constraint further raises the lower bounds on the cross sections, so that they vary through just over 3 (under 2) orders of magnitude in the
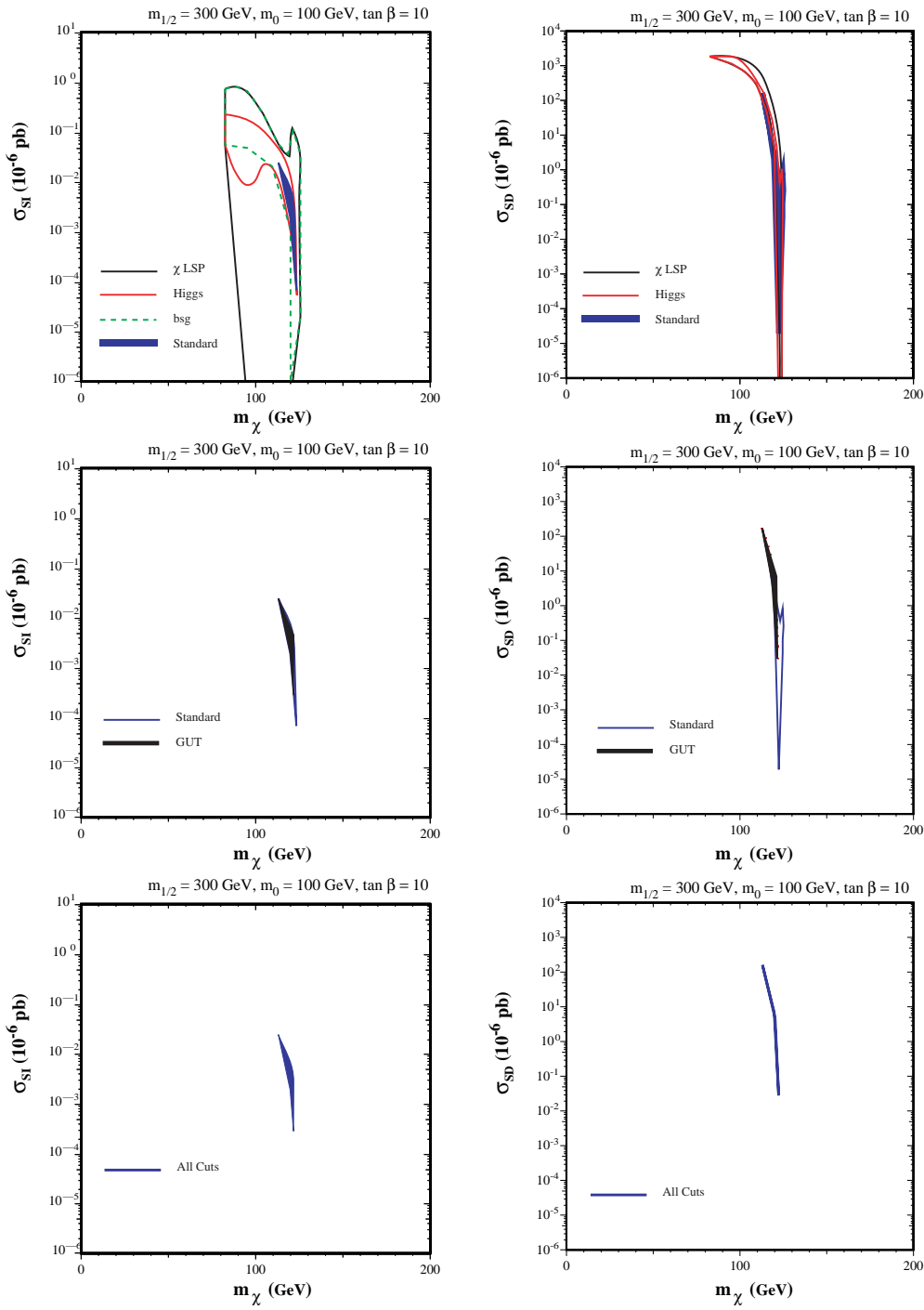
13

Figure 5: *Cross sections allowed in a slice through the NUHM parameter space provided by the (μ, m_A) plane for $\tan \beta = 10$ and $m_{1/2} = 300$ GeV, $m_0 = 100$ GeV. The selections of points in the different panels are the same as in Fig. 4, as are their indications. In addition, panel (a) also shows the $b \to s\gamma$ cut (dashed lines).*

spin-(in)dependent case.

Notice that there is an isolated point at $m_\chi \sim 80$ GeV. This corresponds to a very narrow region just to the right of the chargino mass-bound line in Fig. 3(a,c) at $\mu \sim 120$ GeV, $M_2 \sim 240$ GeV, which is not visible because of the plotting resolution. What happens is that as μ decreases, m_χ falls below the m_h threshold, and hence the annihilation cross section decreases leading to an acceptable value of $\Omega_\chi h^2$. However, as μ decreases further, neutralino-chargino coannihilation becomes stronger, suppressing $\Omega_\chi h^2$ again to be less than 0.1.

This brief survey shows the importance of implementing correctly the GUT stability constraint, which may (in different cases) bound the cross sections either above or below. As many authors have previously pointed out in the CMSSM case, the $g_\mu - 2$ constraint is also potentially important. In certain cases, it can also strengthen significantly the lower limits on the NUHM cross sections.

4.2   General Analysis

Equipped with the above information about some specific examples, we now make a general analysis of the possible values of the elastic scattering cross sections. In the first place, we concentrate on the case $\tan\beta = 10$, but relaxing the previous restricted choices of other parameters that we took as examples. To produce the plots, we generate random points (about 30000 points for each plot) within the following ranges:

$$100 \text{ GeV} \leq m_{1/2} \leq 1500 \text{ GeV},$$
$$0 \leq m_0 \leq 1000 \text{ GeV},$$
$$-2000 \text{ GeV} \leq \mu \leq 2000 \text{ GeV},$$
$$90 \text{ GeV} \leq m_A \leq 1500 \text{ GeV}. \tag{6}$$

We first impose the same standard experimental and phenomenological constraints discussed earlier, namely: a consistent electroweak vacuum, $0.1 < \Omega_\chi h^2 < 0.3$, $m_h > 114$ GeV and the $b \to s\gamma$ constraint. In a previous paper on the CMSSM [3], we rescaled the elastic scattering cross sections for models that predicted $\Omega_\chi h^2 < 0.1$ by the factor $\Omega_\chi h^2/0.1$, so as to account for the fact that the neutralino could constitute at most this fraction of the galactic halo. In the results that follow, we show how this rescaling affects the upper limits on the cross sections. Next we apply the GUT stability cut, and finally we show the implications of imposing the cut on $g_\mu - 2$. The resulting ranges of the elastic scattering cross sections for $\tan\beta = 10$ are displayed in Fig. 7.

We note that the spin-independent cross section shown in Fig. 7(a) may be as large as
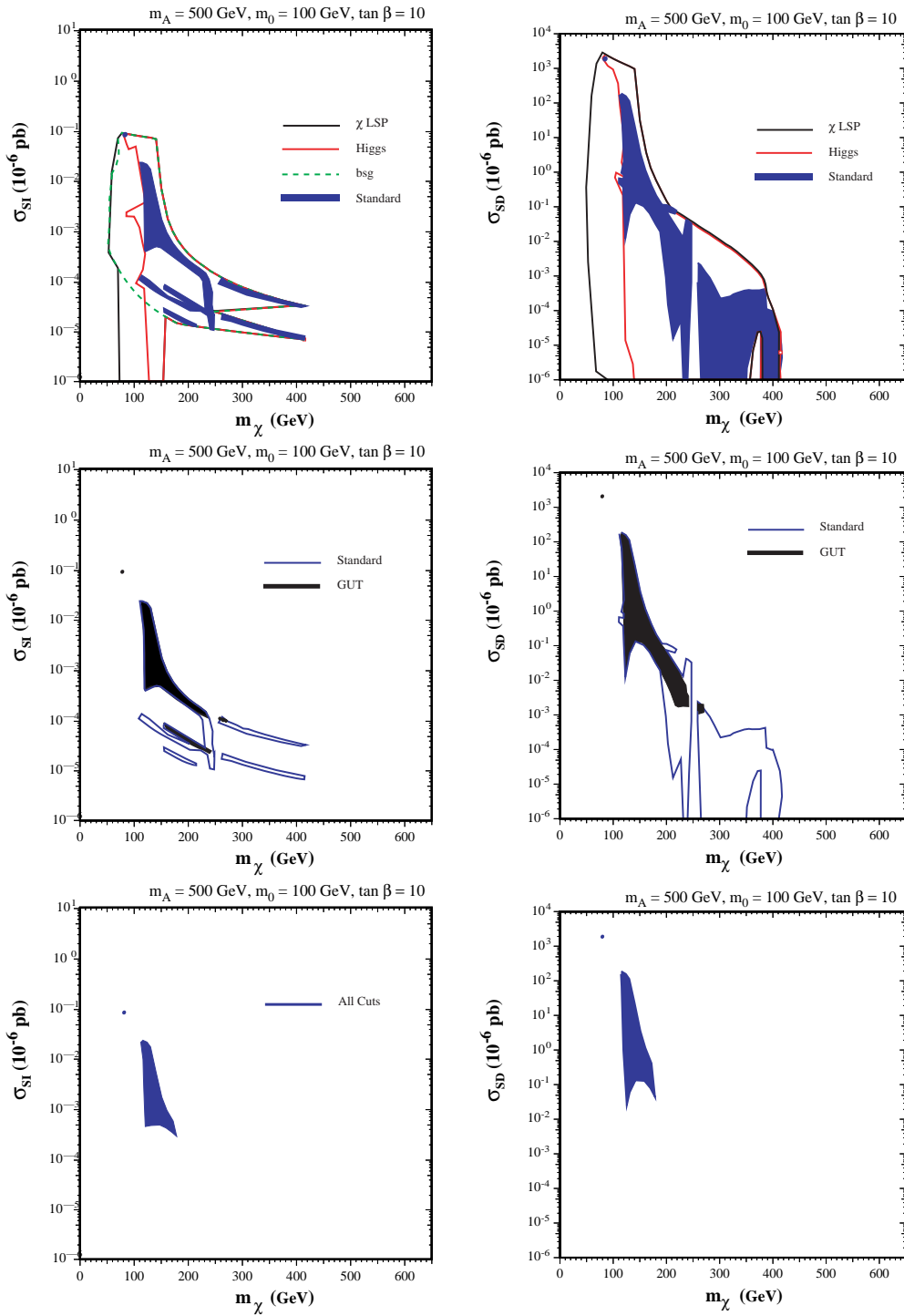
Figure 6: *Cross sections allowed in a slice through the NUHM parameter space provided by the (μ, M_2) plane for $\tan\beta = 10$ and $m_0 = 100$ GeV, $m_A = 500$ GeV. The selections of points in the different panels are the same as in Fig. 5, as are their indications.*
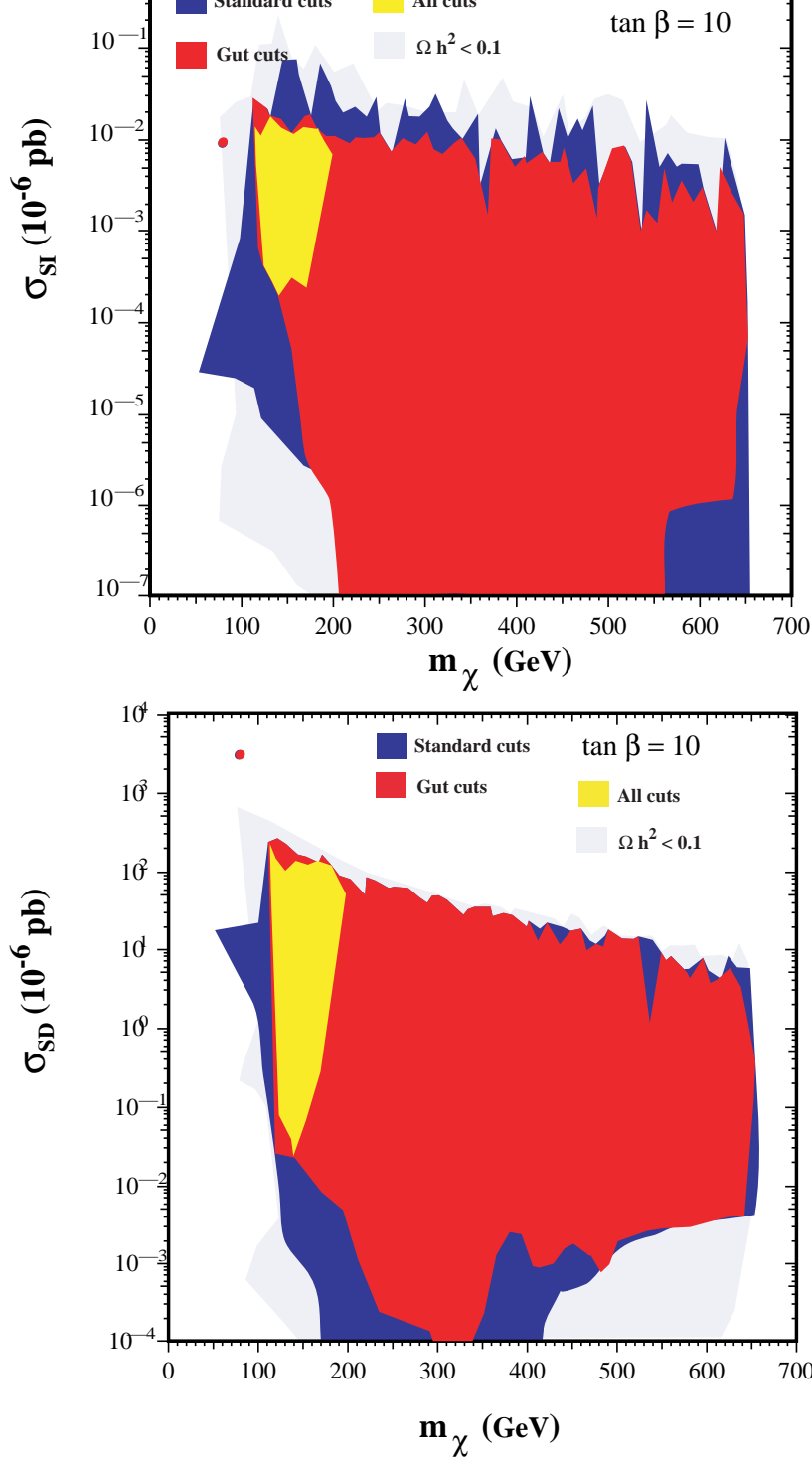
Figure 7: *Ranges of (a) the spin-independent and (b) the spin-dependent cross sections for* $\tan\beta = 10$. *The ranges allowed by the standard cuts on* $\Omega_\chi h^2$, m_h *and* $b \to s\gamma$ *have dark shading, those still allowed by the GUT stability cut have medium shading, and those still allowed after applying all the cuts including* $g_\mu - 2$ *have light shading. The pale shaded region corresponds to the extra area of points with low relic densities, whose cross sections have been rescaled appropriately.*

17

a few $\times 10^{-8}$ pb, decreasing only slightly as m_χ increases, whilst values lower than 10^{-13} pb cannot be excluded. The raggedness of the upper limit on the cross section reflects the fact that our sampling produced very few points with such large cross sections: values in between the crags cannot be excluded, but must be very rare. Between the crags there are valleys, below which the density of points is significantly larger. The lowest values of the cross section occur for $\mu < 0$, where cancellations are possible in the spin-independent scattering matrix element, as discussed in a previous paper [2]. The GUT stability constraints exclude some low cross-section values at both small and large m_χ, but do not provide an overall lower bound. It does however, lower the upper bound by as much as a factor of about 5. Negative μ, and hence very low cross-section values, would be excluded by the putative $g_\mu - 2$ constraint, as shown in Fig. 7(a). For $\mu > 0$, we find (not shown) spin-independent cross sections only above 10^{-11} pb.

Fig. 7(a) also displays the region (pale shaded) which survives all standard cuts, except that $\Omega h^2 < 0.1$. For points in this region, we have rescaled the cross section by a factor of $\Omega h^2/0.1$, to allow for the fact that the LSP could not in this case make up all the cold dark matter in the Universe, and hence *a fortiori* in the galactic halo. As one can see, many of the spaces between the crags are now filled in with such points, but very few give significantly larger cross sections.

In the case of the spin-dependent cross section shown in Fig. 7(b), the upper limit is better defined, and decreases monotonically from $\sim 3 \times 10^{-3}$ pb for $m_\chi \sim 80$ GeV to $\sim 5 \times 10^{-6}$ pb for $m_\chi \sim 650$ GeV. Cross sections lower than $\sim 10^{-10}$ pb are possible for either sign of μ, even after imposing the GUT stability cuts. In this case, the points with rescaled cross sections enhance the cross section by a factor of about 3 at low neutralino masses.

The isolated point in both panels at $m_\chi \sim 80$ GeV now corresponds to a narrow region around $\mu \sim -110$ GeV and large $m_A > 1000$ GeV, which is between the $m_h = 114$ GeV and $m_{\chi^\pm} = 103.5$ GeV lines. Its existence is very sensitive to the implementation of the Higgs mass bound.

We note that the ranges allowed by $g_\mu - 2$ are relatively restricted. For a start, we find that 110 GeV $\lesssim m_\chi \lesssim$ 200 GeV. Moreover, even within this range, very low cross-section values are excluded. Overall, we find ranges between $\sim 2 \times 10^{-8}$ pb and $\sim 2 \times 10^{-10}$ pb for the spin-independent cross section, and between $\sim 2 \times 10^{-4}$ pb and $\sim 2 \times 10^{-8}$ pb for the spin-independent cross section.

Ranges for the spin-independent and -dependent cross sections for $\tan\beta = 20$ are shown in Fig. 8. Looking first at the spin-independent cross section in panel (a), we see that our standard cuts on $m_h, \Omega_\chi h^2$ and $b \to s\gamma$ would allow somewhat larger values than for

$\tan \beta = 10$. This difference is less marked when the GUT stability cut is also applied, except for some exceptional parameter choices at small m_χ. The jaggedness of the peaks is more pronounced at this value of $\tan \beta$. Once again, we emphasize that while we do not expect the area between the peaks to be empty, the density of points there is extremely low. When one keeps the low-relic-density points (rescaled appropriately), we see that indeed the crags are filled in to some extent. For $\tan \beta = 20$ these points do not enhance the cross section significantly. The values of m_χ allowed by $g_\mu - 2$ are larger for $\tan \beta = 20$ than for $\tan \beta = 10$, and lower cross sections are also attainable. Overall, the spin-independent cross section may vary between $\sim 3 \times 10^{-7}$ pb and 10^{-10} pb when $\tan \beta = 20$.

In the case of the spin-dependent cross section shown in Fig. 8(b), the upper and lower bounds for $\tan \beta = 20$ are very similar to those for $\tan \beta = 10$ if only the standard and GUT cuts are applied. However, slightly lower values of the cross section are allowed when the $g_\mu - 2$ constraint is applied, without a strong dependence on the value of m_χ (which may be somewhat larger than in the case of $\tan \beta = 10$). For $\tan \beta = 20$, the spin-dependent cross section ranges between $\sim 2 \times 10^{-3}$ pb and $\sim 10^{-8}$ pb.

Continuing now to $\tan \beta = 35$, as shown in Fig. 9, we see again that the spin-independent cross section may be somewhat larger still than for $\tan \beta = 20$, though the same is not true for the spin-dependent cross sections. Once again, the $g_\mu - 2$ constraint allows larger values of m_χ as $\tan \beta$ is increased, opening up the possibility of a smaller cross section, particularly in the spin-dependent case where a cancellation may occur, potentially suppressing the cross section by a couple of orders of magnitude. Both these tendencies are accentuated in the case $\tan \beta = 50$, as shown in Fig. 10. For both $\tan \beta = 35, 50$, the spin-independent cross section may, in some exceptional cases, rise above 10^{-6} pb, even after implementing all the cuts. It may also drop as low as 10^{-10} pb. The maximal spin-dependent cross section is above 10^{-4} pb in the $\tan \beta = 35$ case, and somewhat below 10^{-4} pb in the $\tan \beta = 50$ case. In both cases, it may also drop as low as 10^{-10} pb.

Finally, in Fig. 11, we display the allowed ranges of (a) the spin-independent and (b) the spin-dependent cross sections when we sample randomly $\tan \beta$ as well as the other NUHM parameters. We see no big surprises compared with the previous plots for individual values of $\tan \beta$, but observe that the boundaries of the shaded regions are very ragged, reflecting the finite sample size. After incorporating all the cuts, including that motivated by $g_\mu - 2$, we find that the spin-independent cross section has the range 10^{-6} pb $\gtrsim \sigma_{SI} \gtrsim 10^{-10}$ pb, and the spin-dependent cross section has the range 10^{-4} pb $\gtrsim \sigma_{SD} \gtrsim 10^{-10}$ pb, with somewhat larger (smaller) values being possible in exceptional cases. If the $g_\mu - 2$ cut is removed, the upper limits on the cross sections are unchanged, but much lower values become possible:
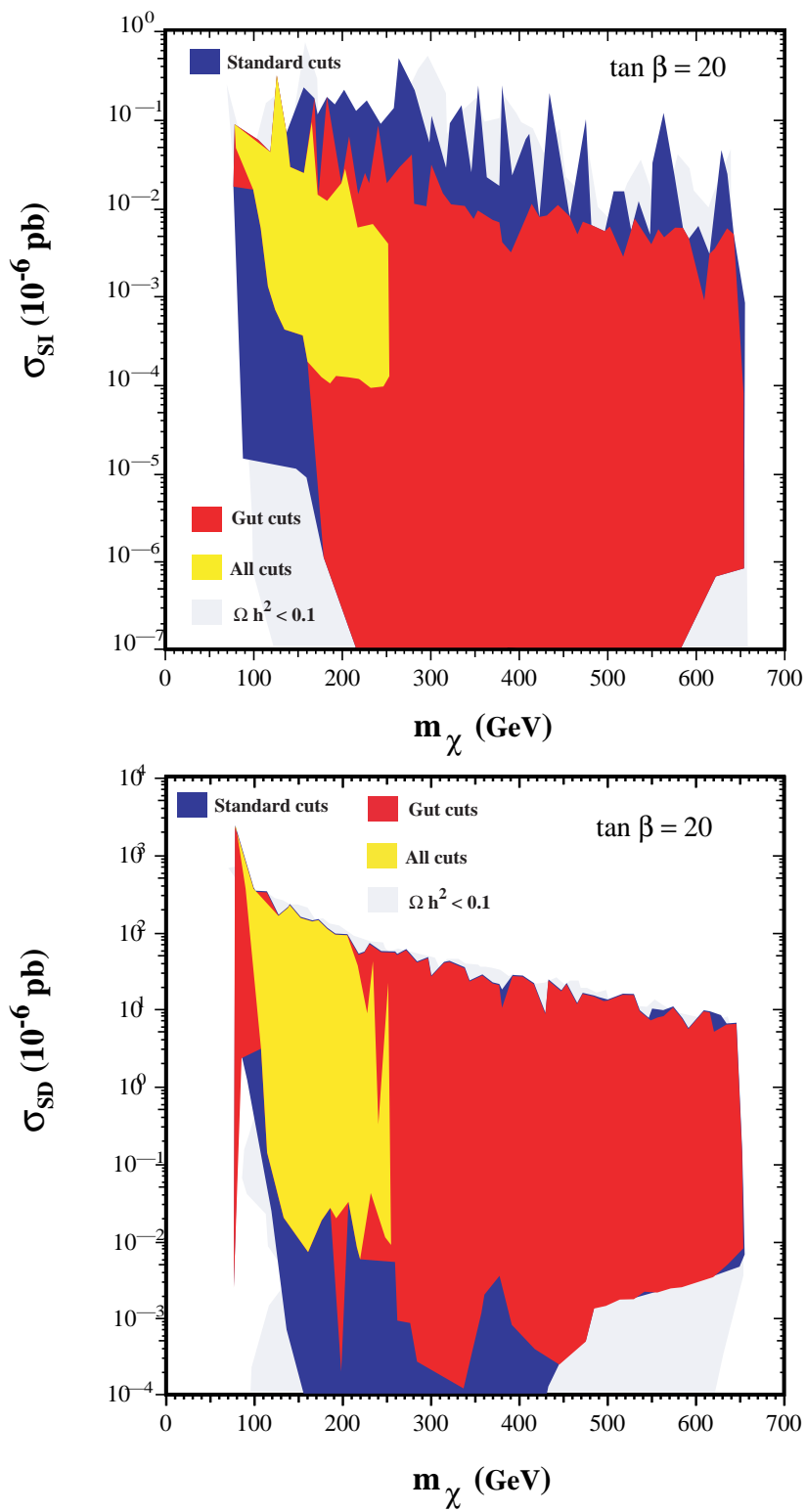
Figure 8: *Ranges of (a) the spin-independent and (b) the spin-dependent cross sections for* $\tan\beta = 20$. *The shadings are the same as in Fig. 7.*
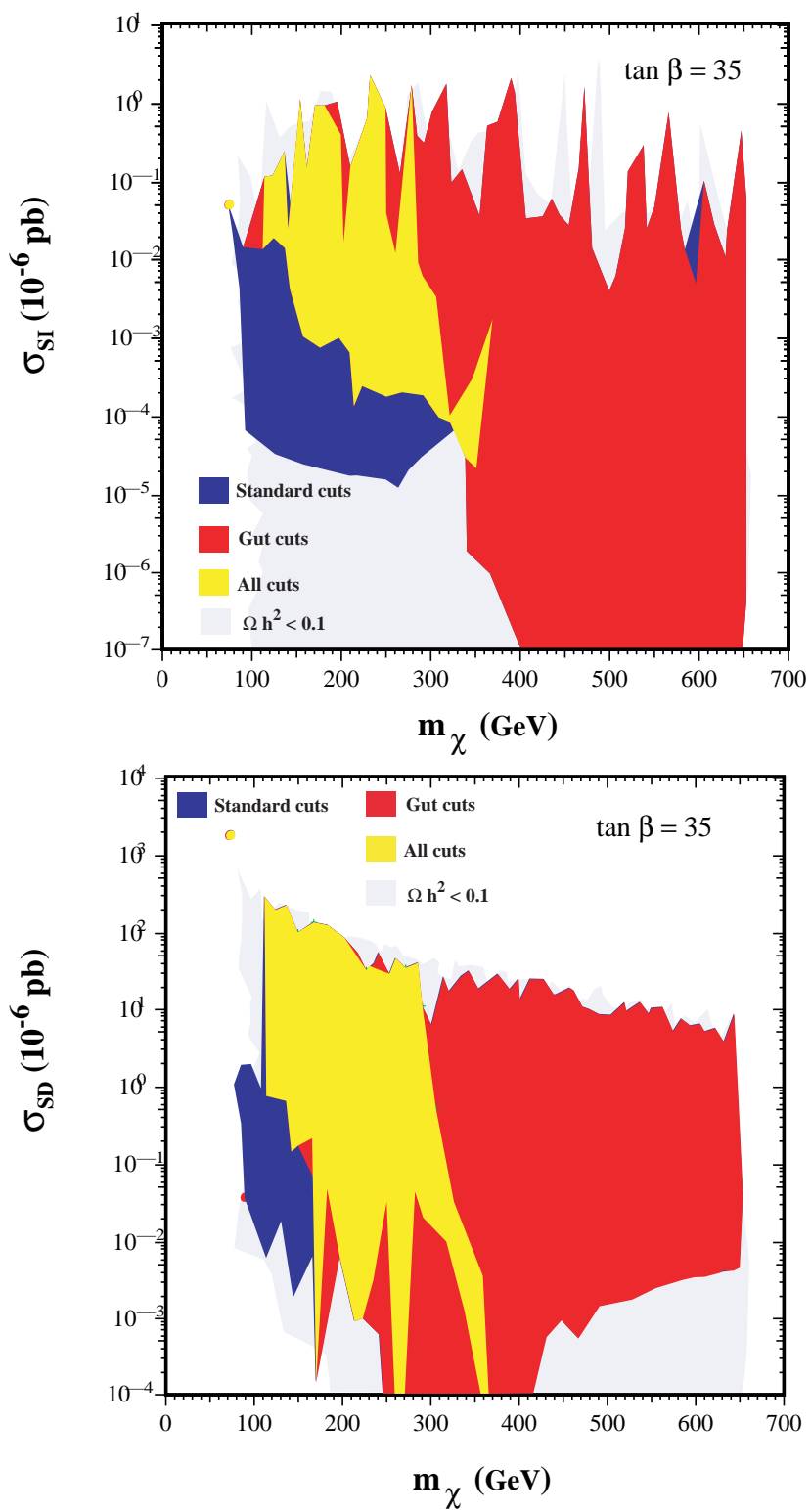
Figure 9: *Ranges of (a) the spin-independent and (b) the spin-dependent cross sections for* $\tan \beta = 35$. *The shadings are the same as in Fig. 7.*
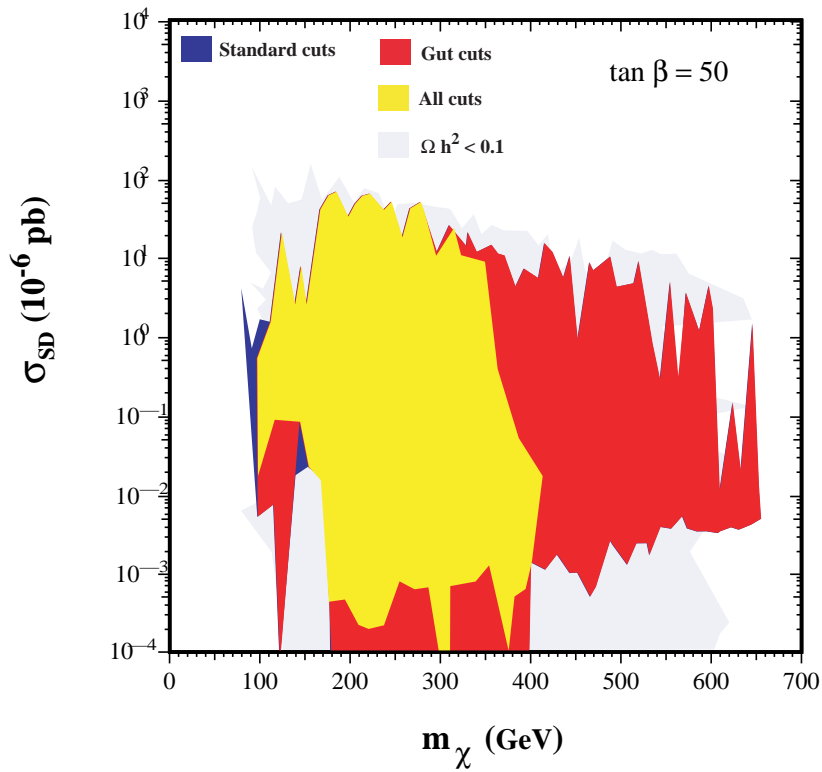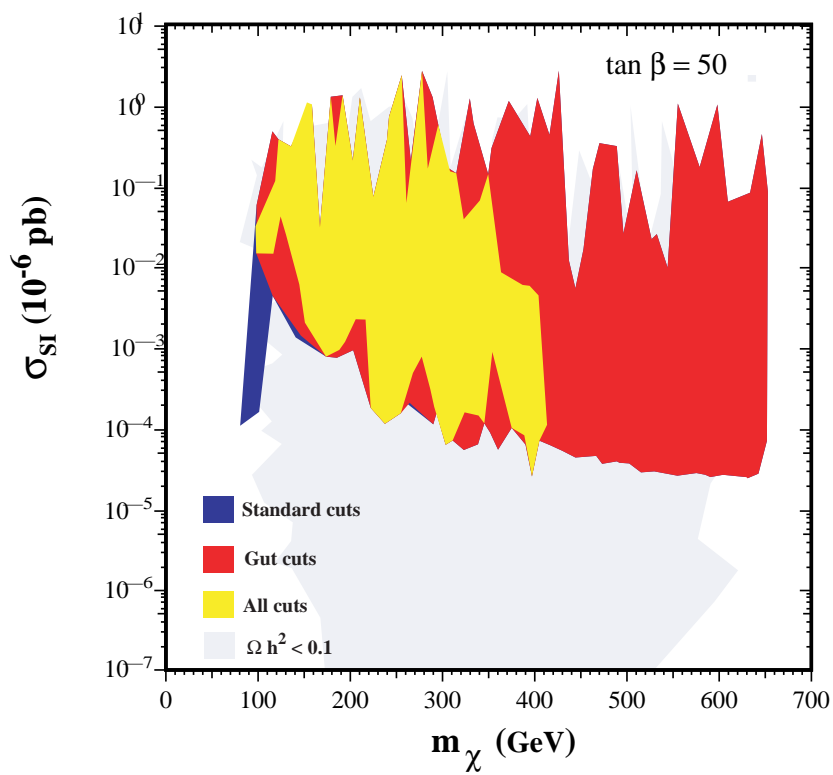
Figure 10: *Ranges of (a) the spin-independent and (b) the spin-dependent cross sections for* $\tan\beta = 50$. *The shadings are the same as in Fig. 7.*

$\sigma_{SI} \ll 10^{-13}$ pb and $\sigma_{SD} \ll 10^{-10}$ pb.

5   Conclusions

We have discussed in this paper the possible ranges of spin-(in)dependent elastic cross sections in the NUHM, in which the input soft supersymmetry-breaking masses of the Higgs doublets are allowed to differ from those of the squarks and sleptons - which are still assumed to be universal. Fig. 11 summarizes the results, including the flexibility of varying $\tan \beta$ as well as the input scalar and fermion masses $m_{0,1/2}$, the Higgs mixing parameter μ and the the pseudoscalar Higgs mass m_A. In this paper, we have not varied the trilinear soft supersymmetry-breaking parameter A, whose effective low-energy value has in any case a limited range when renormalized from the GUT scale downwards, so that it does not have a large effect on the cross sections we study.

We have stressed in this paper the importance of incorporating consistently all the available phenomenological constraints from laboratory experiments and cosmology. We have also stressed the importance of taking into account the running of the NUHM parameters over the full range of scales between the GUT scale and the electroweak scale. As we have discussed explicitly, the requirement that the effective scalar potential be stable at the GUT scale restricts the allowed variations in the non-universalities of the soft supersymmetry-breaking Higgs masses.

The effects of our phenomenological cuts and this GUT stability requirement can be seen in Fig. 11, and also in the previous Figs. 7, 8, 9 and 10 for $\tan \beta = 10, 20, 35$ and 50, respectively. Some examples of our analysis for specific slices through the NUHM parameter space can be seen in earlier figures.

In general, we find that cross sections may differ by a few orders of magnitude from those found in the CMSSM, in which the soft supersymmetry-breaking Higgs masses are assumed to be universal with the slepton and squark masses at the GUT scale. However, the spin-independent cross section normally lies well below the present experimental sensitivity. Only in a few exceptional cases do we find a cross section as large as the present experimental sensitivity $\sigma_{SI} \sim 10^{-6}$ pb, and a sensitivity $\sigma_{SI} \sim 10^{-10}$ pb would be required to cover most of the preferred domain of NUHM parameter space. Even this sensitivity would be insufficient if one disregards the indication from $g_\mu - 2$, which is the only constraint that motivates a useful upper bound on the sparticle mass scale, and hence a useful lower bound on σ_{SI}. In the case of the spin-dependent cross section, values of σ_{SD} as low as $\sim 10^{-10}$ pb cannot be excluded even if one takes seriously the $g_\mu - 2$ constraint.
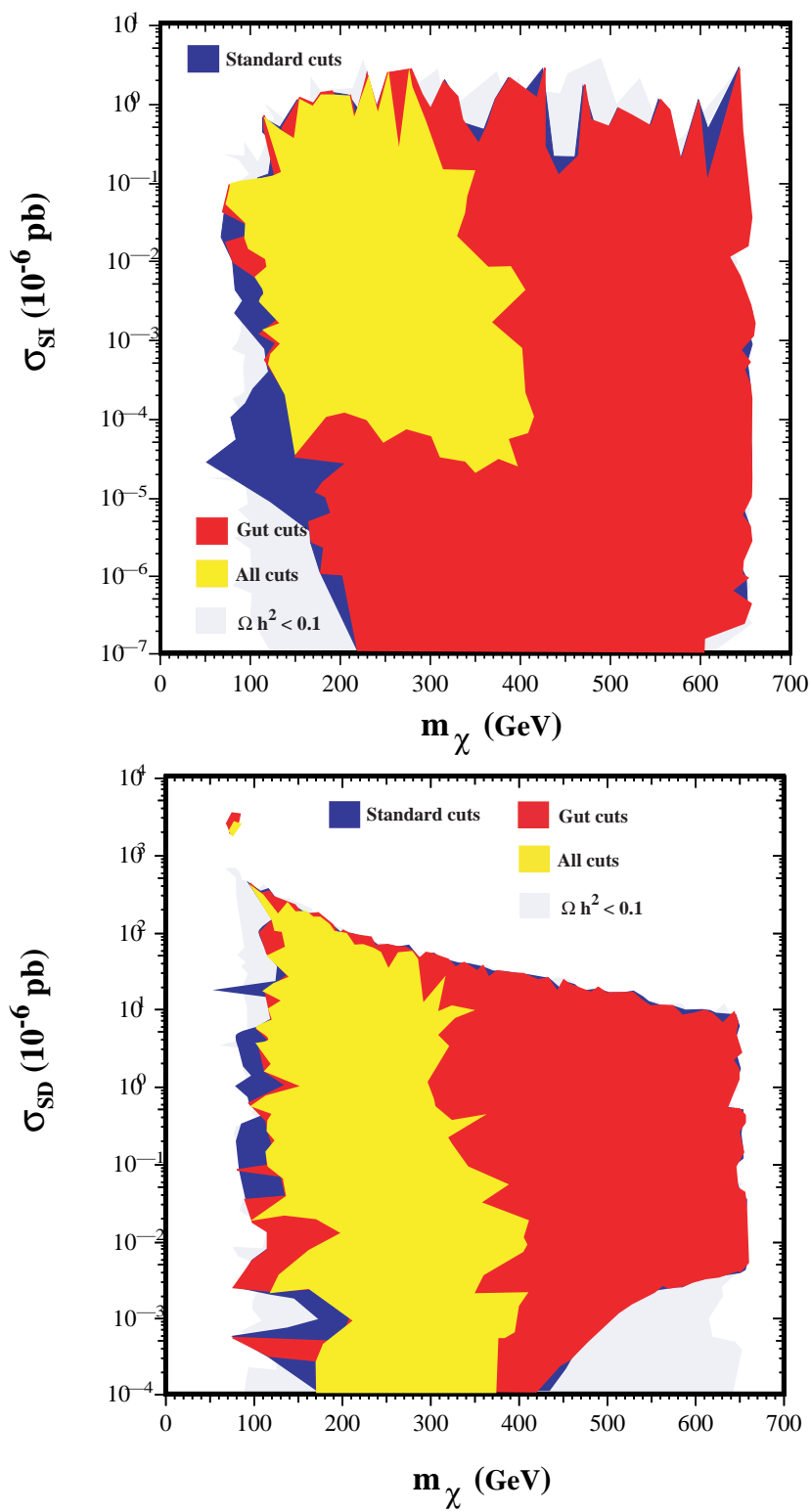
Figure 11: *Ranges of (a) the spin-independent and (b) the spin-dependent cross sections, sampling randomly all allowed values of* $\tan\beta$. *The shadings are the same as in Fig. 7.*

24

The next logical step in the exploration of the MSSM, relaxing further the assumption of full scalar-mass universality as in the CMSSM, is to allow the soft supersymmetry-breaking slepton and squark masses to differ at the GUT scale. The allowed ranges of the effective low-energy slepton and squark masses, after renormalization, will be restricted by analogues of the GUT stability constraints we have applied in this paper. In particular, we note that general choices of the effective low-energy slepton and squark masses may lead (in particular) to tachyonic squarks below the GUT scale, when renormalized to higher scales. We will explore in future publications the effects on the parameter space and the ranges of cross sections of applying consistently the GUT stability constraints to the general non-universal MSSM.

Acknowledgments

References

[1] K. Griest, Phys. Rev. D **38**, 2357 (1988); J. Ellis and R. Flores, Nucl. Phys. B **307**, 883 (1988); R. Barbieri, M. Frigeni and G. Giudice, Nucl. Phys. B **313**, 725 (1989); R. Flores, K.A. Olive and M. Srednicki, Phys. Lett. B **237**, 72 (1990); J. Ellis and R. Flores, Phys. Lett. B **263**, 259 (1991); J. Ellis and R. Flores, Phys. Lett. B **300**, 175 (1993); M. Drees and M. M. Nojiri, Phys. Rev. D **48**, 3483 (1993); V. Bednyakov, H.V. Klapdor-Kleingrothaus and S. Kovalenko, Phys. Rev. D **50**, 7128 (1994); R. Arnowitt and P. Nath, Phys. Rev. D **54**, 2374 (1996) [arXiv:hep-ph/9509260]; L. Bergstrom and P. Gondolo, Astropart. Phys. **5**, 263 (1996) [arXiv:hep-ph/9510252]. H. Baer and M. Brhlik, Phys. Rev. D **57**, 567 (1998) [arXiv:hep-ph/9706509]; E. Accomando, R. Arnowitt, B. Dutta and Y. Santoso, Nucl. Phys. B **585**, 124 (2000) [arXiv:hep-ph/0001019]; A. Corsetti and P. Nath, Phys. Rev. D **64** (2001) 125010 [arXiv:hep-ph/0003186].

[2] J. Ellis, A. Ferstl and K. A. Olive, Phys. Lett. B **481**, 304 (2000) [arXiv:hep-ph/0001005].

[3] J. Ellis, A. Ferstl and K. A. Olive, Phys. Rev. D **63**, 065016 (2001) [arXiv:hep-ph/0007113].

[4] J. R. Ellis, J. L. Feng, A. Ferstl, K. T. Matchev and K. A. Olive, Eur. Phys. J. C **24**, 311 (2002) [arXiv:astro-ph/0110225].

[5] J. R. Ellis, A. Ferstl and K. A. Olive, Phys. Lett. B **532**, 318 (2002) [arXiv:hep-ph/0111064].

[6] For other scattering calculations, see, for example: J. L. Feng, K. T. Matchev and F. Wilczek, Phys. Lett. B **482** (2000) 388 [arXiv:hep-ph/0004043]; A. Bottino, F. Donato, N. Fornengo and S. Scopel, Phys. Rev. D **63**, 125003 (2001) [arXiv:hep-ph/0010203]; M. Drees, Y. G. Kim, T. Kobayashi and M. M. Nojiri, Phys. Rev. D **63**, 115009 (2001) [arXiv:hep-ph/0011359]; Y. G. Kim and M. M. Nojiri, arXiv:hep-ph/0104258; A. B. Lahanas, D. V. Nanopoulos and V. C. Spanos, Mod. Phys. Lett. A **16**, 1229 (2001) [arXiv:hep-ph/0009065]; A. B. Lahanas, D. V. Nanopoulos and V. C. Spanos, Phys. Lett. B **518**, 94 (2001) [arXiv:hep-ph/0107151]; E. A. Baltz and P. Gondolo, Phys. Rev. Lett. **86**, 5004 (2001) [arXiv:hep-ph/0102147]; Y. G. Kim, T. Nihei, L. Roszkowski and R. Ruiz de Austri, JHEP **0212**, 034 (2002) [arXiv:hep-ph/0208069]; M. E. Gómez and J. D. Vergados, Phys. Lett. B **512**, 252 (2001) [arXiv:hep-ph/0012020].

[7] J. Ellis, J.S. Hagelin, D.V. Nanopoulos, K.A. Olive and M. Srednicki, Nucl. Phys. B **238** (1984) 453; see also H. Goldberg, Phys. Rev. Lett. **50** (1983) 1419.

[8] A. Melchiorri and J. Silk, Phys. Rev. D **66** (2002) 041301 [arXiv:astro-ph/0203200].

[9] M. Drees, M. M. Nojiri, D. P. Roy and Y. Yamada, Phys. Rev. D **56** (1997) 276 [Erratum-ibid. D **64** (1997) 039901] [arXiv:hep-ph/9701219]; see also M. Drees, Y. G. Kim, M. M. Nojiri, D. Toya, K. Hasuko and T. Kobayashi, Phys. Rev. D **63** (2001) 035008 [arXiv:hep-ph/0007202].

[10] V. Berezinsky, A. Bottino, J. R. Ellis, N. Fornengo, G. Mignola and S. Scopel, Astropart. Phys. **5** (1996) 1 [arXiv:hep-ph/9508249]; P. Nath and R. Arnowitt, Phys. Rev. D **56** (1997) 2820 [arXiv:hep-ph/9701301]; A. Bottino, F. Donato, N. Fornengo and S. Scopel, Phys. Rev. D **59** (1999) 095004 [arXiv:hep-ph/9808459]; Phys. Rev. D **63**, 125003 (2001) [arXiv:hep-ph/0010203]; R. Arnowitt, B. Dutta and Y. Santoso, Nucl. Phys. B **606** (2001) 59 [arXiv:hep-ph/0102181]; V. Bertin, E. Nezri and J. Orloff, arXiv:hep-ph/0210034.

[11] J. R. Ellis, T. Falk, G. Ganis, K. A. Olive and M. Schmitt, Phys. Rev. D **58** (1998) 095002 [arXiv:hep-ph/9801445]; J. R. Ellis, T. Falk, G. Ganis and K. A. Olive, Phys. Rev. D **62** (2000) 075010 [arXiv:hep-ph/0004169].

[12] J. R. Ellis, K. A. Olive and Y. Santoso, Phys. Lett. B **539** (2002) 107 [arXiv:hep-ph/0204192].

[13] J. R. Ellis, T. Falk, K. A. Olive and Y. Santoso, arXiv:hep-ph/0210205.

[14] V. D. Barger, M. S. Berger and P. Ohmann, Phys. Rev. D **49** (1994) 4908 [arXiv:hep-ph/9311269].

[15] W. de Boer, R. Ehret and D. I. Kazakov, Z. Phys. C **67** (1995) 647 [arXiv:hep-ph/9405342].

[16] M. Carena, J. R. Ellis, A. Pilaftsis and C. E. Wagner, Nucl. Phys. B **625** (2002) 345 [arXiv:hep-ph/0111245].

[17] L. E. Ibáñez, C. Lopez and C. Munoz, Nucl. Phys. B **256** (1985) 218.

[18] S. P. Martin and M. T. Vaughn, Phys. Rev. D **50** (1994) 2282 [arXiv:hep-ph/9311340].

[19] T. Falk, K. A. Olive, L. Roszkowski and M. Srednicki, Phys. Lett. B **367** (1996) 183 [arXiv:hep-ph/9510308]; A. Riotto and E. Roulet, Phys. Lett. B **377** (1996) 60 [arXiv:hep-ph/9512401]; A. Kusenko, P. Langacker and G. Segre, Phys. Rev. D **54** (1996) 5824 [arXiv:hep-ph/9602414]; T. Falk, K. A. Olive, L. Roszkowski, A. Singh and M. Srednicki, Phys. Lett. B **396** (1997) 50 [arXiv:hep-ph/9611325].

[20] T. Falk, K. A. Olive and M. Srednicki, Phys. Lett. B **339** (1994) 248 [arXiv:hep-ph/9409270].

[21] Joint LEP 2 Supersymmetry Working Group, *Combined LEP Chargino Results, up to 208 GeV*,
http://lepsusy.web.cern.ch/lepsusy/www/inos_moriond01/charginos_pub.html.

[22] Joint LEP 2 Supersymmetry Working Group, *Combined LEP Selectron/Smuon/Stau Results, 183-208 GeV*,
http://lepsusy.web.cern.ch/lepsusy/www/sleptons_summer02/slep_2002.html.

[23] LEP Higgs Working Group for Higgs boson searches, OPAL Collaboration, ALEPH Collaboration, DELPHI Collaboration and L3 Collaboration, *Search for the Standard Model Higgs Boson at LEP*, ALEPH-2001-066, DELPHI-2001-113, CERN-L3-NOTE-2699, OPAL-PN-479, LHWG-NOTE-2001-03, CERN-EP/2001-055, arXiv:hep-ex/0107029; *Searches for the neutral Higgs bosons of the MSSM: Preliminary combined results using LEP data collected at energies up to 209 GeV*, LHWG-NOTE-2001-04, ALEPH-2001-057, DELPHI-2001-114, L3-NOTE-2700, OPAL-TN-699, arXiv:hep-ex/0107030; LHWG Note/2002-01, http://lephiggs.web.cern.ch/LEPHIGGS/papers/July2002_SM/index.html.

[24] Y. Okada, M. Yamaguchi and T. Yanagida, Prog. Theor. Phys. **85** (1991) 1; J. R. Ellis, G. Ridolfi and F. Zwirner, Phys. Lett. B **257** (1991) 83; H. E. Haber and R. Hempfling, Phys. Rev. Lett. **66** (1991) 1815.

[25] S. Heinemeyer, W. Hollik and G. Weiglein, Comput. Phys. Commun. **124** (2000) 76 [arXiv:hep-ph/9812320]; S. Heinemeyer, W. Hollik and G. Weiglein, Eur. Phys. J. C **9** (1999) 343 [arXiv:hep-ph/9812472].

[26] M.S. Alam et al., [CLEO Collaboration], Phys. Rev. Lett. **74** (1995) 2885 as updated in S. Ahmed et al., CLEO CONF 99-10; BELLE Collaboration, BELLE-CONF-0003, contribution to the 30th International conference on High-Energy Physics, Osaka, 2000. See also K. Abe *et al.*, [Belle Collaboration], [arXiv:hep-ex/0107065]; L. Lista [BaBar Collaboration], [arXiv:hep-ex/0110010]; K. Chetyrkin, M. Misiak and M. Munz, Phys. Lett. B **400** (1997) 206 [Erratum-ibid. B **425**, 414 (1997)] [hep-ph/9612313]; T. Hurth, hep-ph/0106050; C. Degrassi, P. Gambino and G. F. Giudice, JHEP **0012** (2000) 009 [arXiv:hep-ph/0009337]; M. Carena, D. Garcia, U. Nierste and C. E. Wagner, Phys. Lett. B **499** (2001) 141 [arXiv:hep-ph/0010003]. P. Gambino and M. Misiak, Nucl. Phys. B **611** (2001) 338; D. A. Demir and K. A. Olive, Phys. Rev. D **65** (2002) 034007 [arXiv:hep-ph/0107329].

[27] G. W. Bennett *et al.* [Muon g-2 Collaboration], Phys. Rev. Lett. **89** (2002) 101804 [Erratum-ibid. **89** (2002) 129903] [arXiv:hep-ex/0208001].

[28] M. Davier, S. Eidelman, A. Hocker and Z. Zhang, arXiv:hep-ph/0208177; see also K. Hagiwara, A. D. Martin, D. Nomura and T. Teubner, arXiv:hep-ph/0209187; F. Jegerlehner, unpublished, as reported in M. Krawczyk, Acta Phys. Polon. B **33** (2002) 2621 [arXiv:hep-ph/0208076].

[29] G. Jungman, M. Kamionkowski and K. Griest, *Phys. Rept.* **267**, 195 (1996);
http://t8web.lanl.gov/people/jungman/neut-package.html.